
Turbulent Cosmic-Ray Reacceleration and the Curved Radio Spectrum of the Radio Relic in the Sausage Cluster

Yutaka FUJITA¹, Hiroki AKAMATSU,² and Shigeo S. KIMURA³

¹Department of Earth and Space Science, Graduate School of Science, Osaka University, Toyonaka, Osaka 560-0043, Japan

²SRON Netherlands Institute for Space Research, Sorbonnelaan 2, 3584 CA Utrecht, The Netherlands

³Frontier Research Institute for Interdisciplinary Sciences, Tohoku University, Sendai 980-8578, Japan and Astronomical Institute, Tohoku University, Sendai 980-8578, Japan

*E-mail: fujita@vega.ess.sci.osaka-u.ac.jp

Received ; Accepted

Abstract

It has often been thought that the northern radio relic in the galaxy cluster CIZA J2242.8+5301 (the “Sausage” Cluster) is associated with cosmic ray (CR) electrons that are accelerated at a shock through the diffusive shock acceleration (DSA) mechanism. However, recent radio observations have shown that the radio spectrum is curved, which is inconsistent with the prediction of a simple DSA model. Moreover, the CR electron spectrum before being affected by radiative cooling seems to be too hard for DSA. In this study, we show that these facts are natural consequences if the electrons are reaccelerated in turbulence downstream of the shock. In this model, DSA is not the main mechanism for generating high-energy electrons. We find that the mean free path of the electrons should be much shorter than the Coulomb mean free path for efficient reacceleration. The scale of the turbulent eddies must be smaller than the width of the relic. We also predict hard X-ray spectra of inverse Compton scattering of photons.

Key words: cosmic rays — galaxies: clusters: individual (CIZA J2242.8+5301) — shock waves — turbulence

1 Introduction

Radio relics are synchrotron emissions often found on the periphery of clusters of galaxies. From their positions and prolonged shapes, they have been associated with cosmic ray (CR) electrons accelerated at shocks in the intracluster medium (ICM). In fact, shocks have been discovered at some relics by X-ray observations (Finoguenov et al. 2010; Macario et al. 2011; Akamatsu et al. 2012a; Akamatsu et al. 2012b; Akamatsu & Kawahara 2013; Ogreaan & Brügggen 2013; Bourdin et al. 2013). It has often been believed that the CR electrons are accelerated at the shocks through the diffusive shock accel-

ation (DSA) mechanism, which is first-order Fermi acceleration (e.g. Roettiger et al. 1999; Fujita & Sarazin 2001; Kang et al. 2012; Yamazaki & Loeb 2015). However, recent observations have shown that the acceleration is much more complicated than expected. For example, the radio spectrum of the relic in the galaxy cluster 1RXS J0603.3 +4214 (“Toothbrush” cluster) is hard and curved, which contradicts predictions based on a simple DSA model (van Weeren et al. 2012; Stroe et al. 2016). Moreover, XMM-Newton observations showed that the position of the shock does not coincide with that of the relic (Ogreaan et al. 2013), although the shock-relic offset was not

recognized in deeper Chandra observations (van Weeren et al. 2016).

In Fujita et al. (2015), we showed that the discrepancies are solved if electrons are reaccelerated in turbulence *downstream* of the shock. In this model, the electrons are first accelerated at a shock through the DSA, although the efficiency does not have to be high. Then, the seed CR electrons are efficiently reaccelerated in the turbulence through second-order Fermi acceleration. Turbulent reacceleration has been studied to explain the origin of giant radio halos observed in clusters (e.g. Schlickeiser et al. 1987; Brunetti et al. 2001; Petrosian 2001; Fujita et al. 2003). Fujita et al. (2015) showed that it can also be applied to radio relics. Turbulent (re)acceleration behind shocks has been considered for objects such as supernova remnants (e.g. Inoue et al. 2010; Zhang 2015) and the Fermi bubbles (e.g. Mertsch & Sarkar 2011; Sasaki et al. 2015).

While the relic in the Toothbrush Cluster has a complicated shape and the Mach number of the associated shock is small ($\mathcal{M} \lesssim 2$; Itahana et al. 2015), the northern relic in the cluster CIZA J2242.8+5301 (the ‘‘Sausage’’ Cluster; $z = 0.1921$) has a clear bow-like shape (van Weeren et al. 2010) and the Mach number is relatively large ($\mathcal{M} \sim 3$; Akamatsu et al. 2015). This may indicate that the DSA model is preferable. However, even this ‘‘textbook’’ example of a relic has a hard, curved radio spectrum, which is not easy to reconcile with DSA models (Stroe et al. 2016). We note that there are modified DSA models in which fossil electrons upstream of the shock are reaccelerated at the shock through DSA (e.g. Kang & Ryu 2015) or magnetic fields vary (Donnert et al. 2016). These could result in a curved radio spectrum. In addition, the impact of the Sunyaev-Zeldovich effect on the radio spectrum could not be ignored (Basu et al. 2015). However, in this study, we attempt to apply our reacceleration model to the relic in the Sausage Cluster in order to solve the contradictions. We do not go into the details of the micro-physics of turbulent reacceleration (e.g., the cascade of turbulence, plasma instabilities, and so on), which are highly unknown at present. Instead, we focus on finding out the parameters that are consistent with observations. The results will be helpful when more comprehensive models are constructed in the future.

2 Models

In the model of Fujita et al. (2015), electrons are first accelerated at a shock through DSA. The momentum spectrum of the accelerated electrons is

$$n_0(p) = A_0 p^{-s}, \quad (1)$$

where p is the electron momentum and A_0 is the normalization. The index is given by

$$s = \frac{r_c + 2}{r_c - 1}, \quad (2)$$

where r_c is the compression ratio:

$$r_c = \frac{(\gamma_g + 1)\mathcal{M}^2}{(\gamma_g - 1)\mathcal{M}^2 + 2}, \quad (3)$$

where $\gamma_g (= 5/3)$ is the adiabatic index, and \mathcal{M} is the Mach number of the shock (e.g. Blandford & Eichler 1987). The downstream density ρ_d and the velocity V_d are related to the upstream density ρ_u and the velocity V_u as $\rho_d = r_c \rho_u$ and $V_d = V_u/r_c$, respectively. We assume that the minimum momentum of the accelerated electrons is $p_{\min} = m_e c$, where m_e is the electron mass, and c is the light velocity. The normalization A_0 in equation (1) is given as follows. The kinetic energy flux upstream of the shock is $\rho_u V_u^2/2$. We assume that a fraction χ_e of the flux is consumed to accelerate electrons. This means that the kinetic energy density of the accelerated CR electrons just downside of the shock is $\epsilon_{e,sh} = \chi_e \rho_u V_u^3/(2V_d) = \chi_e \rho_u V_u^2 r_c/2$. On the other hand, the density is also written as

$$\epsilon_{e,sh} = \int_{p_{\min}}^{\infty} m_e c^2 (\gamma - 1) n_0(p) dp, \quad (4)$$

where γ is the Lorentz factor of a CR electron. From these equations, we obtain

$$A_0 = \frac{\chi_e \rho_u V_u^2 r_c}{2 m_e c^2} / \int_{p_{\min}}^{\infty} (\gamma - 1) p^{-s} dp. \quad (5)$$

We assume that turbulence develops downstream of the shock. The CR electrons accelerated at the shock are swept downstream with the ICM and they are reaccelerated in the turbulence. The evolution of the momentum spectrum $n(t, p)$ on the comoving frame is calculated using the Fokker-Plank equation,

$$\frac{\partial n}{\partial t} - \frac{\partial}{\partial p} \left(p^2 D_{pp} \frac{\partial n}{\partial p} \right) + \frac{\partial}{\partial p} \left(\frac{dp}{dt} n \right) = 0, \quad (6)$$

where D_{pp} is the diffusion coefficient for momentum. The initial spectrum is given by $n(t = 0, p) = n_0(p)$. Since the CR electrons move with the ICM, the distance of the electrons from the shock is written as $x = V_d t$.

We assume that the electrons are scattered by Alfvén waves because they can develop even on small scales through the cascade of turbulence and/or plasma instabilities (see Section 2.2.2 of Brunetti & Jones 2014). Thus, the diffusion coefficient for momentum is

$$D_{pp} \sim \frac{1}{9} p^2 \frac{v_A^2}{D_{xx}}, \quad (7)$$

where v_A is the Alfvén velocity, and D_{xx} is the spatial diffusion coefficient,

$$D_{xx} \sim \frac{c l_{\text{mfp}}}{3}, \quad (8)$$

where l_{mfp} is the mean free path of the electrons (Ohno et al. 2002; see also Isenberg 1987; Schlickeiser 1989; Fujita et al. 2003; Brunetti et al. 2004). The Alfvén velocity is written as $v_A = B_d / \sqrt{4\pi \rho_d}$, where B_d is the downstream magnetic field. When particles are scattered by magnetosonic waves, l_{mfp} may

be comparable to the Coulomb mean free path of thermal particles $l_{\text{mfp},C}$ (e.g. ZuHone et al. 2013; see also Brunetti & Lazarian 2007). However, when they are scattered by Alfvén waves, l_{mfp} may be much smaller than $l_{\text{mfp},C}$. Thus, we assume that l_{mfp} has the form of

$$l_{\text{mfp}}(t, p) = \eta(t)(p/p_0)^{2-q} l_{\text{mfp},C}, \quad (9)$$

where $\eta(t)$ is the reduction factor, p_0 is the reference momentum, and q is the parameter representing the property of the turbulence. The Coulomb mean free path $l_{\text{mfp},C}$ depends on the downstream density ρ_d and temperature T_d . Following Fujita et al. (2015), we set $p_0 = 10^4 m_e c$ and $q = 5/3$ (Kolmogorov case). It is to be noted that even if we adopt $q = 2$ (hard sphere approximation), the results do not change qualitatively. We expect that the turbulence and the Alfvén waves decay with the distance from the shock and we include that effect in $\eta(t)$. Assuming that the decay scale in space is L_t , its time scale is $t_0 = L_t/V_d$. Thus, the reduction factor is represented by

$$\eta(t) = \eta_{\text{min}} \exp(t/t_0). \quad (10)$$

This means that the mean free path increases as CR electrons move away from the shock with the ICM. In equation (6), dp/dt represents cooling of the CR electrons. We include synchrotron, inverse Compton scattering of cosmic microwave background photons, non-thermal bremsstrahlung, and Coulomb interaction (Gould 1975; Sturmer et al. 1997; Sarazin 1999; Yang & Zhang 2009). The synchrotron emission depends on B_d .

3 Results

X-ray observations have shown that the shock parameters for the northern relic in the Sausage Cluster are $V_u = 2300 \text{ km s}^{-1}$, $\mathcal{M} = 2.7$, $\rho_d = 9.4 \times 10^{-28} \text{ cm}^{-3}$, and $T_d = 8.5 \text{ keV}$ (Akamatsu et al. 2015). The Coulomb mean free path downstream of the shock is $l_{\text{mfp},C} \sim 45 \text{ kpc}$. Since the spatial scale of turbulence should be much smaller than the width of the relic ($\sim 100 \text{ kpc}$), we assume that $L_t = 10 \text{ kpc}$ ($t_0 = 12 \text{ Myr}$). We choose the reduction factor at the shock ($\eta_{\text{min}} = 1.6 \times 10^{-7}$), the acceleration efficiency ($\chi_e = 5.0 \times 10^{-7}$), and the downstream magnetic field ($B_d = 0.30 \mu\text{G}$) so that the resultant radio profile and spectrum are consistent with observations (see later). In general, a smaller η_{min} and/or a larger B_d give a larger D_{pp} , which leads to more efficient reacceleration [equations (7)–(10)].

We solve equation (6) assuming that the whole relic is steady. This means that electrons are constantly accelerated at the shock and are reaccelerated in the turbulence. The CR electrons are swept with the ICM and those at a distance x from the shock were located at the shock x/V_d ago. Figure 1 shows the evolution of the CR electron spectrum on the comoving frame. At $t = 0$, the spectrum is given by equation (1) and $s = 2.6$. At $t > 0$, the electrons are reaccelerated in the turbulence and

the number of high-energy electrons ($\gamma \gtrsim 10^4$) increases. Those electrons are responsible for the observed synchrotron emission. The acceleration time scale is given by $t_{\text{acc}} \sim p^2/D_{pp}$, and it is $\sim 8 \text{ Myr}$ at $x = 0$ and $p = p_0$. At $t \gtrsim 20 \text{ Myr}$, the turbulence significantly decays because $t > t_0 = 12 \text{ Myr}$ and then cooling becomes effective. The cooling time is $t_{\text{cool}} \sim p/(dp/dt) \sim 10\text{--}100 \text{ Myr}$ for $\gamma \sim 10^4\text{--}10^5$. Thus, the number of high-energy electrons decreases.

In figure 2, we show the surface brightness at 610 MHz as a function of the projected distance from the shock (x'). For that purpose, we transform the planar shock we implicitly assumed into a curved shock, and then project the radio emission along the line of sight on the sky. Following previous studies, we assume that the shock has a ribbon-like curved surface and it is viewed edge-on with a viewing extension angle of 10° (the total angle subtend is 20° ; van Weeren et al. 2010; Kang & Ryu 2015). The curvature radius is 1.5 Mpc. As can be seen, the model profile reproduces the observations well (van Weeren et al. 2010). At $x = 0$ and $p = p_0$, the spatial scale of the reacceleration is $x_{\text{acc}} = V_d t_{\text{acc}} \sim 7 \text{ kpc}$, which is a factor of a few smaller than the peak position of the surface brightness ($x' \sim 20\text{--}30 \text{ kpc}$) reflecting the increasing $\eta(t)$ [equation (10)]. We note that the slower rise of the radio profile at $x' \gtrsim 0$ does not necessarily mean that our reacceleration model is superior to DSA models. For the latter, the radio emissivity generally has its maximum at the shock ($x = 0$). However, if the shock is curved, the peak position is shifted to $x' > 0$ (see figure 4 in van Weeren et al. 2010). We also show the profile of spectral index α between 153 and 2272 MHz in figure 2. At $x = 0$, the index is $\alpha_{\text{DSA}} = -0.82$, which is the prediction based on the DSA for $\mathcal{M} = 2.7$:

$$\alpha_{\text{DSA}} = \frac{1}{2} - \frac{\mathcal{M}^2 + 1}{\mathcal{M}^2 - 1} \quad (11)$$

(e.g. Blandford & Eichler 1987). At $x' \gtrsim 0$, the index decreases a little because the momentum spectrum at $\gamma \gtrsim 10^4$ is soft at the beginning of reacceleration (see $t = 5 \text{ Mpc}$ in figure 1). Then it starts increasing as the reacceleration proceeds. It would be difficult to observe this dip of the index because of the low surface brightness at $x' \sim 0$ (figure 2). The index reaches the maximum, $\alpha \sim -0.5$, at $x' \sim 20 \text{ kpc}$, around which the surface brightness is also maximized. The maximum index is comparable to observation ($\alpha \sim -0.6$), which is inconsistent with the standard DSA model because it predicts $\mathcal{M} \sim 4.6$ from $\alpha \sim -0.6$ (van Weeren et al. 2010; Stroe et al. 2013). Then, the index and surface brightness gradually decrease owing to the decay of turbulence and cooling.

In figure 3a, we show the radio spectrum of the whole relic and compare it with observations by Stroe et al. (2016). We assume that the length of the relic is 1.7 Mpc and the viewing extension angle is 10° . Our model reproduces the curved spectrum very well, because the momentum spectrum of the CR electrons is not a power law (figure 1). The curved spec-

trum is a natural consequence of second-order Fermi acceleration affected by cooling and a finite acceleration time, which is of the order of t_0 in our case. In figure 3b, we show the broad-band spectra of the relic. The hard X-ray flux from inverse Compton scattering is larger than the synchrotron flux, because the magnetic field of $B_d = 0.30 \mu\text{G}$ is smaller than $B_{\text{CMB}} \approx 3.24(1+z)^2 \mu\text{G} \approx 4.6 \mu\text{G}$, at which synchrotron cooling is comparable to the cooling by inverse Compton scattering.¹ We analyze the Suzaku data of the Sausage Cluster (see Akamatsu et al. 2015) and find that the upper limit of the non-thermal emission is $8.2 \times 10^{-13} \text{ erg s}^{-1}$ in the 0.3–10 keV band, which is consistent with our prediction in figure 3b.

The width of the relic Δx depends on the cooling time of CR electrons. The typical frequency of synchrotron emission from an electron with a Lorentz factor γ in a magnetic field B is $\nu_c \propto \gamma^2 B$. The cooling time of the electron is $t_{\text{cool}} \propto \gamma^{-1} (B^2 + B_{\text{CMB}}^2)^{-1} \propto B^{1/2} \nu_c^{-1/2} (B^2 + B_{\text{CMB}}^2)^{-1}$ (e.g. Rybicki & Lightman 1979). Thus, two values of B give the same t_{cool} for a given ν_c . This means that for a given observation frequency $\nu_{\text{obs}} \sim \nu_c$, there are two values of B that give the same Δx .² For the Sausage Cluster, the value we adopted in figure 3 ($B_d = 0.30 \mu\text{G}$) is the smaller one. Figure 4 is the other solution with the larger magnetic field ($B_d = 9.5 \mu\text{G}$). The other parameters are the same as those for figure 3 except for $\eta_{\text{min}} = 2.9 \times 10^{-4}$, and $\chi_e = 1.5 \times 10^{-8}$. Figure 4a is almost the same as figure 3a. Moreover, we have confirmed that the profiles of surface brightness and spectral index for this large B_d model are almost identical to those in figure 2. On the other hand, the hard X-ray flux in figure 4b is much smaller than that in figure 3b, which can be used to discriminate the high and low B_d models in future observations. Note that in this large B_d model, the spatial diffusion time ($\sim x^2/D_{xx}$) of the CRs is comparable to the advection time ($\sim x/V_d$) around the peak of the surface brightness ($x \sim 20\text{--}30 \text{ kpc}$). Thus, the best fit parameters we obtained above would be somewhat changed if we include the effect of spatial diffusion.

4 Summary and Discussion

In this study, we have shown that turbulent reacceleration of electrons can explain the observed surface brightness profile and the hard, curved radio spectrum of the northern radio relic in the Sausage Cluster. This model also reproduces the properties of the relic in the Toothbrush Cluster

¹ Since the spectra of CR electrons are not represented by a power law (figure 1), the relation between the synchrotron flux, the inverse Compton flux, and the magnetic fields cannot be discussed using the usual formula based on a power-law spectrum (e.g. equation (5.10) in Sarazin 1986).

² Note that the width is not simply given by $\Delta x = V_d t_{\text{cool}}$, which is often assumed when only cooling is important (e.g. van Weeren et al. 2010), because it also depends on the reacceleration of CRs at $x > 0$. Thus, the magnetic field that gives a certain Δx depends on whether reacceleration is considered or not.

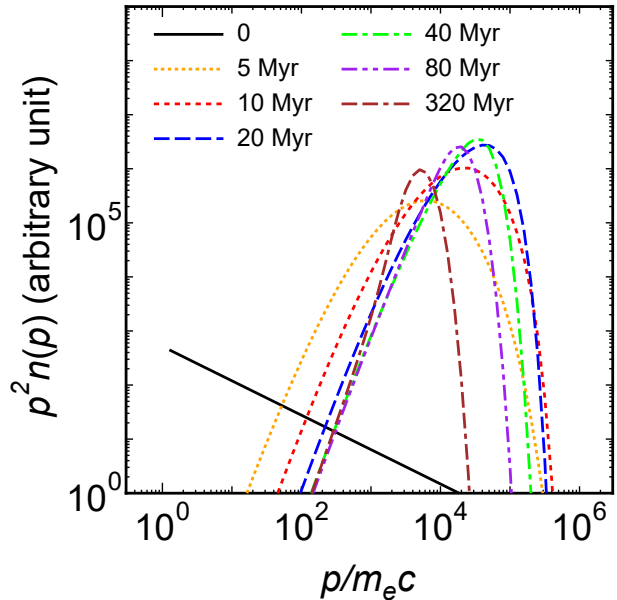


Fig. 1. Electron spectra behind the shock. Time t is shown in the legends; $t = 320 \text{ Myr}$ corresponds to the distance of $x = 266 \text{ kpc}$.

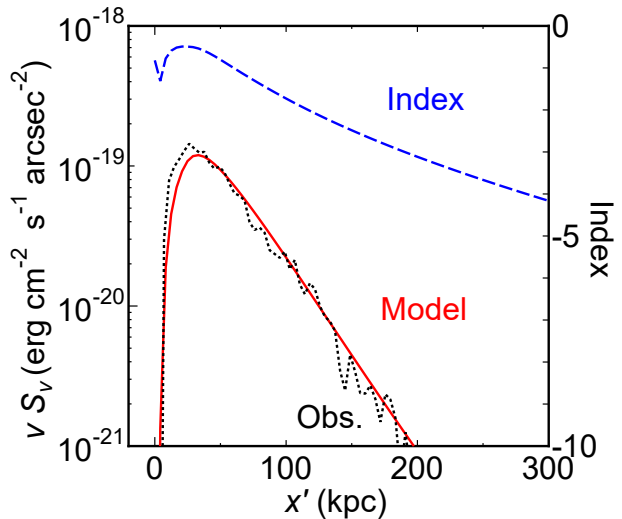


Fig. 2. Synchrotron surface brightness at 610 MHz as a function of the projected distance from the shock. The solid curve is our prediction and the dotted curve is the observation (van Weeren et al. 2010). The normalization of the observed profile is adjusted to be consistent with the total flux (0.2223 Jy) obtained by Stroe et al. (2016). The dashed curve is our prediction for the spectral index between 153 MHz and 2272 MHz.

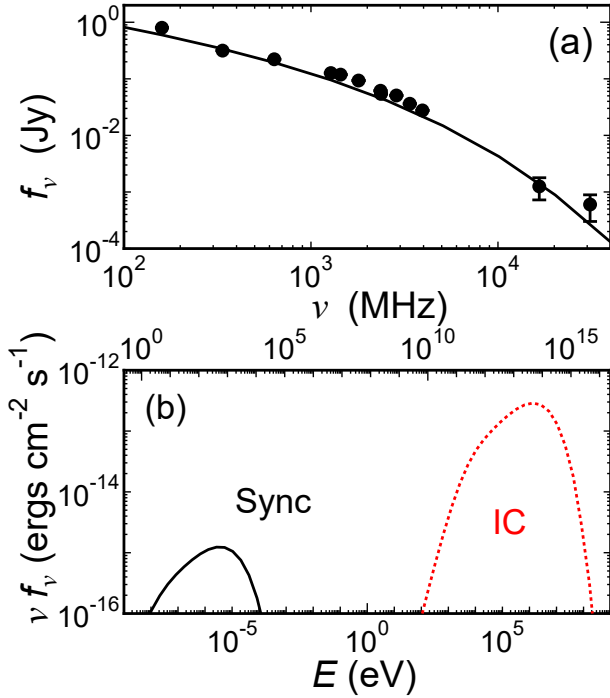


Fig. 3. Results for $B_d = 0.30 \mu\text{G}$, $\eta_{\min} = 1.6 \times 10^{-7}$, and $\chi_e = 5.0 \times 10^{-7}$. (a) Integrated radio spectrum (solid line). Filled circles show the data from Stroe et al. (2016). (b) Broad band spectra. The solid line shows synchrotron emission and the dotted line shows inverse Compton scattering.

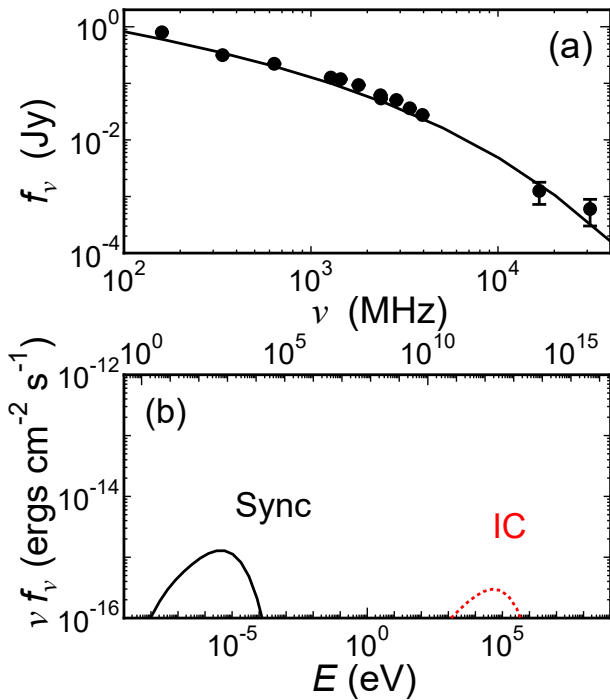


Fig. 4. As figure 3 but for $B_d = 9.5 \mu\text{G}$, $\eta_{\min} = 2.9 \times 10^{-4}$, and $\chi_e = 1.5 \times 10^{-8}$.

(1RXS J0603.3+42141; Fujita et al. 2015). So far, curved radio spectra have been observed for the bright relics in three clusters (Sausage, Toothbrush, and A 2256; Trasatti et al. 2015). This may indicate that the turbulent reacceleration is a fairly common mechanism to create radio relics in clusters. The spatial scale of turbulence must be smaller than the width of the relic and the mean free path of CR electrons must be much shorter than the Coulomb mean free path of thermal particles.

In our model, we assumed that the efficiency of turbulent reacceleration is the highest at the shock front [equation (10)]. However, if it takes some time for eddies to grow up, the turbulent reacceleration starts to develop well behind the shock and the synchrotron emission would clearly be detached from the shock. If this is observed in some relics, it would support our model. Moreover, X-ray observations with a high spectral resolution (e.g., Hitomi, Athena) may reveal turbulence behind shocks.

Some key issues remain unsolved. First, the generation of turbulence needs to be addressed. If a shock travels through inhomogeneous gas, turbulence may be generated (Samtaney & Zabusky 1994; Inoue et al. 2009). In fact, some recent X-ray observations suggest that the ICM in the outskirts of clusters is clumpy (Simionescu et al. 2011). Using numerical simulations, van Weeren et al. (2011) concluded that the amplitude of density fluctuation must be $\lesssim 30$ percent. However, the wavelengths of the fluctuation they studied are rather large (≥ 75 kpc), and the evolution of turbulence when the wavelength is smaller (say 10 kpc) is not certain. Alternatively, if a shock passes through a turbulent region, turbulence could be amplified downstream of the shock (Iapichino & Brüggen 2012). Moreover, some plasma instabilities may be developing and generating turbulence downstream. Second, relics are often polarized (Feretti et al. 2012), which may be incompatible with the turbulent reacceleration model. For the Sausage Cluster, the relic is strongly polarized at the 50 to 60% level (van Weeren et al. 2010). However, compressional amplification of the magnetic field may account for a large polarization of the radio emission (Iapichino & Brüggen 2012). Note that in our model the mean free path associated with the turbulent reacceleration (l_{mfp}) is much larger than the gyro radius of the CR electrons:

$$r_g = \frac{pc}{eB_d} \approx 5.7 \times 10^{13} \left(\frac{p}{10^4 m_e c} \right) \left(\frac{B_d}{0.30 \mu\text{G}} \right)^{-1} \text{ cm}, \quad (12)$$

where e is the elementary charge. In general, the mean free path is represented as $l_{\text{mfp}} \sim r_g (B/\delta B)^2$, where r_g is the gyro radius of a particle, B is the background magnetic field, and δB is the fluctuation of the field (e.g. Longair 1994). Thus, $l_{\text{mfp}} \gg r_g$ means $\delta B/B \ll 1$, which may indicate that the turbulence on the micro-scales is not strong and magnetic fields may be organized enough. If the model with the larger B_d and η_{\min} is realized (figure 4), the fluctuation $\delta B/B$ is even smaller.

Acknowledgments

We thank the anonymous referee for a thorough review and constructive suggestions. We are grateful to R. J. van Weeren for providing us observational data. This work was supported by KAKENHI No. 15K05080 (Y. F.). H. A. is supported by a Grant-in-Aid for Japan Society for the Promotion of Science (JSPS) Fellows (26-606).

References

- Akamatsu, H., de Plaa, J., Kaastra, J., et al. 2012, PASJ, 64, 49
- Akamatsu, H., & Kawahara, H. 2013, PASJ, 65, 16
- Akamatsu, H., Takizawa, M., Nakazawa, K., et al. 2012, PASJ, 64, 67
- Akamatsu, H., van Weeren, R. J., Ogreaan, G. A., et al. 2015, A&A, 582, A87
- Basu, K., Vazza, F., Erler, J., & Sommer, M. 2015, arXiv:1511.03245
- Blandford, R., & Eichler, D. 1987, Phys. Rep., 154, 1
- Bourdin, H., Mazzotta, P., Markevitch, M., Giacintucci, S., & Brunetti, G. 2013, ApJ, 764, 82
- Brunetti, G., Blasi, P., Cassano, R., & Gabici, S. 2004, MNRAS, 350, 1174
- Brunetti, G., & Jones, T. W. 2014, International Journal of Modern Physics D, 23, 1430007
- Brunetti, G., & Lazarian, A. 2007, MNRAS, 378, 245
- Brunetti, G., Setti, G., Feretti, L., & Giovannini, G. 2001, MNRAS, 320, 365
- Donnert, J. M. F., Stroe, A., Brunetti, G., Hoang, D., & Roettgering, H. 2016, arXiv:1603.06570
- Feretti, L., Giovannini, G., Govoni, F., & Murgia, M. 2012, A&AR, 20, 54
- Finoguenov, A., Sarazin, C. L., Nakazawa, K., Wik, D. R., & Clarke, T. E. 2010, ApJ, 715, 1143
- Fujita, Y., & Sarazin, C. L. 2001, ApJ, 563, 660
- Fujita, Y., Takizawa, M., & Sarazin, C. L. 2003, ApJ, 584, 190
- Fujita, Y., Takizawa, M., Yamazaki, R., Akamatsu, H., & Ohno, H. 2015, ApJ, 815, 116
- Gould, R. J. 1975, ApJ, 196, 689
- Inoue, T., Yamazaki, R., & Inutsuka, S. 2009, ApJ, 695, 825
- Inoue, T., Yamazaki, R., & Inutsuka, S.-i. 2010, ApJL, 723, L108
- Iapichino, L., & Brügggen, M. 2012, MNRAS, 423, 2781
- Isenberg, P. A. 1987, J. Geophys. Res., 92, 1067
- Itahana, M., Takizawa, M., Akamatsu, H., et al. 2015, PASJ, 67, 113
- Kang, H., Ryu, D., & Jones, T. W. 2012, ApJ, 756, 97
- Kang, H., & Ryu, D. 2015, ApJ, 809, 186
- Longair M. S., 1994, High Energy Astrophysics, Vol. 2, 2nd edn. Cambridge Univ. Press, Cambridge. Section 20.4
- Macario, G., Markevitch, M., Giacintucci, S., et al. 2011, ApJ, 728, 82
- Mertsch, P., & Sarkar, S. 2011, Physical Review Letters, 107, 091101
- Ogreaan, G. A., & Brügggen, M. 2013, MNRAS, 433, 1701
- Ogreaan, G. A., Brügggen, M., van Weeren, R. J., et al. 2013, MNRAS, 433, 812
- Ohno, H., Takizawa, M., & Shibata, S. 2002, ApJ, 577, 658
- Petrosian, V. 2001, ApJ, 557, 560
- Roettiger, K., Burns, J. O., & Stone, J. M. 1999, ApJ, 518, 603
- Rybicki G. B., & Lightman, A. P. 1979, Radiative Processes in Astrophysics (New York: Wiley)
- Samtaney R., & Zabusky N. J., 1994, J. Fluid Mech., 269, 45
- Sarazin, C. L. 1986, Reviews of Modern Physics, 58, 1
- Sarazin, C. L. 1999, ApJ, 520, 529
- Sasaki, K., Asano, K., & Terasawa, T. 2015, ApJ, 814, 93
- Schlickeiser, R. 1989, ApJ, 336, 243
- Schlickeiser, R., Sievers, A., & Thiemann, H. 1987, A&A, 182, 21
- Simionescu, A., Allen, S. W., Mantz, A., et al. 2011, Science, 331, 1576
- Stroe, A., Shimwell, T., Rumsey, C., et al. 2016, MNRAS, 455, 2402
- Stroe, A., van Weeren, R. J., Intema, H. T., et al. 2013, A&A, 555, A110
- Sturmer, S. J., Skibo, J. G., Dermer, C. D., & Mattox, J. R. 1997, ApJ, 490, 619
- Trasatti, M., Akamatsu, H., Lovisari, L., et al. 2015, A&A, 575, A45
- van Weeren, R. J., Brunetti, G., Brügggen, M., et al. 2016, arXiv:1601.06029
- van Weeren, R. J., Brügggen, M., Röttgering, H. J. A., & Hoeft, M. 2011, MNRAS, 418, 230
- van Weeren, R. J., Röttgering, H. J. A., Brügggen, M., & Hoeft, M. 2010, Science, 330, 347
- van Weeren, R. J., Röttgering, H. J. A., Intema, H. T., et al. 2012, A&A, 546, A124
- Yamazaki, R., & Loeb, A. 2015, MNRAS, 453, 1990
- Yang, X. C., & Zhang, L. 2009, A&A, 496, 751
- Zhang, M. 2015, ApJ, 812, 148
- ZuHone, J. A., Markevitch, M., Brunetti, G., & Giacintucci, S. 2013, ApJ, 762, 78